The Journal of Chemical Physics

Structure effects on electrocatalysts. Oxygen reduction on Te-modified Pt(111) surfaces: Site-blocking vs electronic effects

Cite as: J. Chem. Phys. **152**, 134702 (2020); https://doi.org/10.1063/5.0003125
Submitted: 04 February 2020 . Accepted: 10 March 2020 . Published Online: 03 April 2020

Ana María Gómez-Marín, Valentín Briega-Martos, and Juan M. Feliu

The Journal of Chemical Physics ARTICLE scitation.org/journal/jcp

Structure effects on electrocatalysts. Oxygen reduction on Te-modified Pt(111) surfaces: Site-blocking vs electronic effects

Cite as: J. Chem. Phys. 152, 134702 (2020); doi: 10.1063/5.0003125
Submitted: 4 February 2020 • Accepted: 10 March 2020 •
Published Online: 3 April 2020

Ana María Gómez-Marín,[1,a)] Valentín Briega-Martos,[2] and Juan M. Feliu[2,a)]

AFFILIATIONS

[1] Department of Chemistry, Division of Fundamental Sciences (IEF), Technological Institute of Aeronautics (ITA), São José dos Campos CEP: 12228-900, SP, Brazil

[2] Instituto de Electroquímica, Universidad de Alicante, Apt 99, E-03080 Alicante, Spain

Note: This paper is part of the JCP Special Topic on Interfacial Structure and Dynamics for Electrochemical Energy Storage.
[a)] **Authors to whom correspondence should be addressed:** agomezma@ita.br. **Tel.:** +55 12 3947 6852 and juan.feliu@ua.es. **Tel.:** +34 965 909 301. **Fax:** +34 965 903 537

ABSTRACT

In this work, the oxygen reduction reaction (ORR) on tellurium-modified Pt(111) surfaces has been studied. Adsorption of Te adatoms on Pt(111) progressively shifts toward less positive values of both the ORR reaction onset and the half-wave potential in 0.1M $HClO_4$ for $0 < \theta_{Te} < 0.25$. However, at $\theta_{Te} > 0.25$, the ORR activity increases relative to the one at $\theta_{Te} < 0.25$, but remains lower than that on clean Pt(111). Results were analyzed in light of simulations of kinetic currents as a function of θ_{Te}, calculated by employing a simple mean field model including both site blocking and electronic effects. Inside this framework, experimental data are best explained by considering that oxygenated Te species inhibit the ORR by either negatively modifying adsorption energies of reaction intermediates or combined site-blocking and electronic effects. A redox ORR catalysis due to redox properties of Te adatoms is discarded. Contrarily, in 0.05M H_2SO_4, a positive catalytic effect has been found, interpreted in terms of a competitive adsorption–desorption mechanism involving the replacement of adsorbed sulfate by Te adatoms. On the other hand, despite the strong site-blocking effect on H_{ads} and OH_{ads} adsorption by Te adatoms, it appears that the reduced Te–Pt(111) adlayer does not inhibit the reaction, suggesting different active sites for H_{ads} and OH_{ads} adsorption and for the rate-determining step of the ORR mechanism.

I. INTRODUCTION

Chemical modification of electrode surfaces can have important consequences for catalytic reactions and charge-transfer processes at electrified interfaces, and thus, it is one of the most common methods for the design of new materials and electrocatalysts for different applications, such as fuel cell technology. Additionally, the adsorption of foreign atoms on metal surfaces is also an attractive strategy to change surface properties of an electrode in a relatively controlled way[1–3] and get insights into the chemical environment of electrode surfaces at the atomic level during electrochemical reactions, such as the adlayer's structure and available surface sites.[4–7] This is an essential information for the identification of catalytic active sites, or composition of actives centers, and, in general, for revealing complex relationships between the surface structure and catalytic reactivity.[8,9]

In this sense, the electrochemical dynamics and electrocatalytical properties of platinum single crystals modified by either irreversible adsorption[1,2,10–12] or underpotential deposition (UPD)[4,8,13–16] of foreign adatoms have been extensively studied in the past years, especially for the oxidation of organic molecules such as carbon monoxide,[17,18] formic acid,[18–22] methanol,[18,23,24] and ethanol oxidation.[21,25] In the first method, irreversible adsorption of foreign adatoms can be simply achieved by either continuously cycling the electrode inside a potential region where the adatom is stably adsorbed onto the surface or dipping it into a solution containing the respective soluble ions for short periods of time, until a given coverage is attained. This is because the adlayer of the

foreign atom is spontaneously formed onto the electrode surface upon immersion. Typical examples of foreign adatoms irreversibly adsorbed onto structurally well-defined Pt surfaces are bismuth, selenium, tellurium, and sulfur.[1,2,6,10–12,17,22,25,26]

For the oxygen reduction reaction (ORR), the main cathodic reaction of metal–air batteries and fuel cells, several studies have shown that adatom adsorption can have important consequences for the electrode catalytic activity, depending on the chemical nature of the substrate and adsorbate,[3,4,6,7,15,16,26–29] the supporting electrolyte,[7–9,30–32] and the electrode's crystallographic orientation.[7–9,30,33,34] Initial studies on polycrystalline surfaces demonstrated that foreign metal monolayers, such as Ag, Tl, Cu, Cd, Pb, and Bi, may have a profound catalytic effect on the ORR on Au electrodes,[3,29] while on polycrystalline platinum (PolyPt), inhibitory effects were mainly found,[3] highlighting the inner-sphere character of some of the steps of the ORR mechanism.[3,29] These effects were primarily explained in terms of either a more favorable adsorption of oxygen or oxygen-containing species, as adsorbed hydroxyl (OH_{ads}) or oxygen (O_{ads}), on Au modified than on clean Au surfaces[3] or the emergence of alternative reaction paths.[3,35–37] Examples of the latter case are the existence of a redox catalysis because of adatom's redox properties[3,35,36] and the appearance of new adsorption sites that facilitate the rupture of the O–O bond.[37]

Subsequent studies included the effect of structural aspects on the ORR kinetics by employing single crystals surfaces of different orientations.[4,6–9,15,27,28,30–34] For example, studies on Ag single crystals reported a gradual decrease in the ORR activity by increasing adsorbate coverage due to the formation of adsorbate superlattice structures from Ag(111)–(2 × 2)Me, $\theta_{Me} \approx 0.25$, to Ag(111)–($\sqrt{3} \times \sqrt{3}$)R30°Me, $\theta_{Me} \approx 0.33$, with Me ≡ Pb, Tl.[29,38] In this case, the maximum inhibition effect on the ORR, an inner-sphere reduction process on this surface, occurred as soon as the Ag electrode is screened off completely by the formation of a Ag(111)–3(2 × 2)Me structure.[29]

For the case of Pt single crystals, similar inhibitory effects on the ORR activity have been, in general, reported for Ag,[4] Cu,[15] halides,[5,16,28,34,39] and Bi adatoms.[14] In addition, in this case, a strong effect of the crystallographic orientation on the ORR kinetics is commonly acknowledged in adsorbing electrolytes, such as H_2SO_4 containing solutions,[9,30,32,34,40] but it is not found in non-adsorbing electrolytes.[8,30,33] In some cases, nevertheless, the inhibition level strongly depends on the adatom's coverage and the nature of the Pt-adatom's bond in such a way that even an enhanced ORR activity has been reported either at specific adatom's coverages of cyanide submonolayers on Pt(111)[6,26] or at structurally well-defined Ag_xPt_{1-x}/Pt(111) surface alloys.[41] In most of these studies, changes in the ORR activity have been explained in terms of either direct/indirect electronic effects, such as changes in the potential of zero charge, dipole–dipole interactions, etc., or site-blocking/site availability (ensemble) effects.[4,7,15,28,34,37,39,41,42] However, the reasons for undoubtedly considering either site-blocking or electronic effects are not completely clear, and in many cases, it has also been considered that both mechanisms can simultaneously take place.[6,8,32]

Clearly, metal adatoms adsorbed at the submonolayer level on well-defined electrodes is a common method in electrocatalysis for both altering the catalytic performance and gaining information on the nature of active sites. Within this goal, in this work, the ORR is analyzed on tellurium-modified Pt(111) surfaces in both adsorbing and non-adsorbing electrolytes to provide a better understanding of the relationship between the catalytic activity and surface structure-composition. Results are interpreted in terms of simulations of kinetic currents as a function of the Te-coverage, θ_{Te}, calculated by employing a simple mean field model that includes both site blocking and electronic effects. These electrocatalytic studies on well-defined single crystal surfaces are not only of fundamental interest but also for the development of practical strategies for enhancing electrode activity in strongly adsorbing electrolytes, such as in H_2SO_4 containing solutions.[6,7,26]

II. EXPERIMENTAL DETAILS

Electrodes with (111) surface orientation, prepared from small Pt beads, ~2–3 mm in diameter following standard procedures,[43] were used as working electrodes. All the experiments were carried out at room temperature and performed in a two-compartment, three-electrode all-glass cell following an experimental protocol detailed elsewhere.[44] Prior to each experiment, electrodes were flame-annealed in a gas–oxygen flame, cooled down in a reductive H_2/Ar (1:3) atmosphere, and transferred to the cell protected by a drop of ultrapure water saturated with this mixture of gases. Solutions were prepared from perchloric acid (Merck, p.a.), ultrapure water (Purelab Ultra 18.2 MΩ cm^{-1}, Elga-Vivendi), and TeO_2 (Sigma-Aldrich). H_2, O_2, and Ar (N50, Air Liquide) were also employed. All potentials were measured against a Reversible Hydrogen Electrode (RHE), and a large, flame-cleaned, Pt wire coil was used as a counter electrode.

The irreversible adsorption of tellurium on Pt(111) single-crystals has been described elsewhere.[1] Adsorption was performed either by putting the electrode surface in contact with a TeO_2 containing solution (10^{-5}–10^{-3}M) in 0.1M $HClO_4$ for short periods of time (5–60 s) or by cycling the electrode in those solutions few times in a potential region where Te atoms adsorbed on the electrode are stable (0.05 V–0.9 V).[1] The modified electrode was then rinsed with Milli-Q water and immersed again in the other electrochemical cell containing only the test electrolyte at 0.1 V, where the adlayer is stable. Then, the voltammetric profile was recorded. Regardless of the adsorption procedure employed, similar current–potential, *i*–*E*, profiles are recorded in both cases at equivalent Te-coverages.

Oxygen reduction measurements on Pt (111) surfaces under convective regime were performed with the hanging meniscus rotating disk electrode (HMRDE) configuration[45] by using an electrode holder for bead-type single-crystal electrodes adapted to Radiometer Analytical EDI-101. The electrode was placed in the holder so that its surface was perpendicular and centered to the rotation axis (as much as possible). Voltammetric scans were collected at freshly annealed surfaces, cycled first in the low potential region to verify their quality, as well as the cleanliness of the surface. The stability of the voltammetric profiles with time was carefully checked to ensure solution cleanliness, especially during HMRDE experiments, owing to forced convection.

III. RESULTS AND DISCUSSION

A. Tellurium adlayers on Pt(111)

Prior to the study of catalytic properties of tellurium modified Pt(111) surfaces, Te–Pt(111), toward the ORR, main voltammetric features of modified electrodes in oxygen-free solutions will be described. Figure 1 resumes the current density–potential, *j*–*E*, profiles of Te–Pt(111) electrodes in Ar-saturated 0.1M $HClO_4$ solutions at different tellurium coverages. For the sake of comparison, the voltammetric profile of bare Pt(111) is also given.

Cyclic Voltammetric (CVs) profiles in Fig. 1 agree well with those reported previously.[1] For bare Pt(111) electrodes, the nature of interfacial processes between 0.06 V and 1.0 V has been well described before, and only a brief picture will be presented. The hydrogen adsorption–desorption process, giving rise to the broad current signal at low potentials, between ~0.06 V and 0.4 V, is separated from the so-called "butterfly" feature, attributed to hydroxyl adsorption–desorption from water dissociation among ~0.55 V–0.85 V, by a small double layer region ~0.45 V–0.55 V.

The electrochemical response of Te modified Pt(111) electrodes is similar to the one recorded in other cases in which irreversible adatom adsorption on Pt(111) takes place.[10–12] Comparison of CVs of bare and Te-modified Pt(111) surfaces at Te-coverages lower than 0.25, $\theta_{Te} < 0.25$, shown in Figs. 1(a)–1(c), clearly illustrates that as the tellurium coverage increases, both the hydrogen, H_{ads}, and hydroxyl, OH_{ads}, coverages decrease, and a new voltammetric signal at ~0.83 V appears, which proportionally increases with θ_{Te}. The reversibility of this couple of peaks is practically independent of $\theta_{Te} < 0.25$, although a small increase in the positive and negative peak potentials is noted at increasing coverages, from 0.814 and 0.808 V at $\theta_{Te} \sim 0.05$ to 0.839 and 0.826 V at $\theta_{Te} \sim 0.21$, respectively.

Cyclic voltammograms depicted in Figs. 1(a)–1(c) for $0 < \theta_{Te} < 0.25$ are stable in the potential region below ~0.95 V,[1,46] indicating that oxidized Te adatoms remain adsorbed on the electrode. At higher potentials, however, a slow oxidative stripping of Te adatoms to soluble species, proposed to be an oxygenated Te^{4+}_{aq} species,[1] takes place, and this dissolution process is accelerated in the presence of dissolved oxygen.[46] At $\theta_{Te} = 0.25$, the current peak at ~0.83 V achieves the maximum integrated charge, and simultaneously, no charge related to hydrogen adsorption/desorption is observed in the CV, which indicates that adsorption sites for H_{ads} have been fully blocked by irreversibly adsorbed Te. This peak has been attributed to the electrochemical oxidation of surface Te adatoms.[1,46–48]

Electrochemical scanning tunneling microscope (STM) measurements for $\theta_{Te} = 0.25$ revealed an ordered $(2 \times \sqrt{3})$-rectangular structure for the oxygenated Te–Pt(111) adlayer, with one Te^{4+} atom and one O^{2-} atom, i.e., $\theta_{Te} = 0.25$ and $\theta_O = 0.25$, and a distance of 3.8 Å between nearest spots, suggesting a dissociative adsorption of the oxygenated Te species in solution.[46,48] Based on this information, an electrochemical process represented by Eq. (1) was proposed in which adsorbed anions from the electrolyte solution would compensate for the net positive charge of the adsorbed Te|O mixed layer,[46,47] as proposed for other metal adlayers on Pt(111),[13]

$$Pt(111) - TeO^{2+}_{ads} + 2H^{+}_{(aq)} + 4e^{-} \leftrightarrow Pt(111) - Te_{(ads)} + H_2O. \quad (1)$$

In agreement, x-ray photoelectron spectroscopy studies have also suggested a change in the Te valence state from Te^0 to Te^{4+}, together with the appearance of adsorbed oxygen, O_{ads}, in the surface after the redox process at 0.83 V during the positive scan has taken place.[47] However, the existence of an adsorbed cation, such as TeO^{2+}_{ads}, on the Pt(111) surface at the potentials where the Te redox process occurs is rather improbable. This is because at those potentials, the Pt(111) surface should bear a positive charge, considering that the potential of zero total charge of the substrate under those experimental conditions is reported to be around 0.3 V.[49] Therefore, it would be more reasonable to propose that the Te redox process on

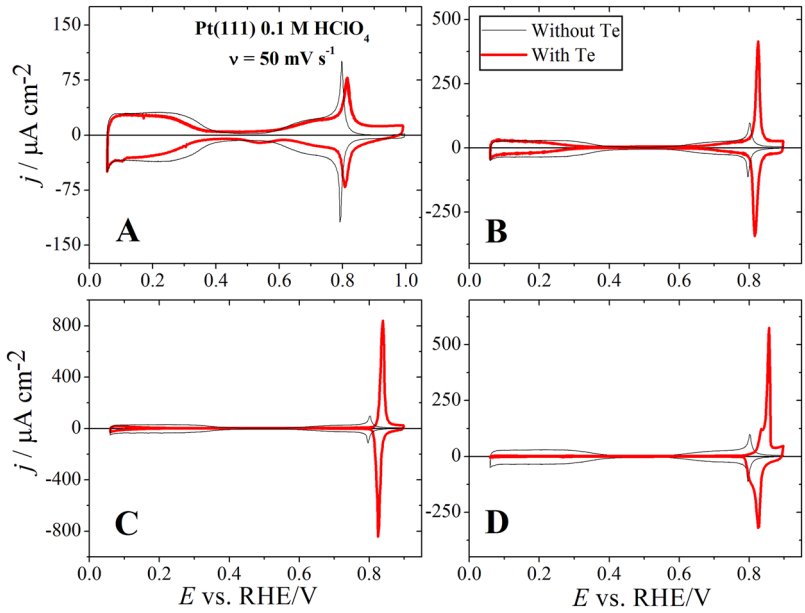

FIG. 1. Voltammetric curve of Te– Pt(111) electrodes at different tellurium coverages: $\theta_{Te} \approx 0.05$ (a), $\theta_{Te} \approx 0.10$ (b), $\theta_{Te} \approx 0.21$ (c), and $\theta_{Te} \approx 0.38$ (d). Voltammetric profile of bare Pt(111) is also given (thin line). Test solution: Ar-saturated 0.1M $HClO_4$. Scan rate: 0.05 V s^{-1}.

the surface would be better represented by[1]

$$Pt(111) - TeO_{2(ads)} + 4H^{+}_{(aq)} + 4e^{-} \leftrightarrow Pt(111) - Te_{(ads)} + 2H_2O. \quad (2)$$

On the other hand, STM measurements for the reduced Te–Pt(111) adlayer have found that Te atoms in the $(2 \times \sqrt{3})$ rectangular array are not stable in the absence of either oxygen[46] or TeO_2 in the solution.[48] Under those conditions, two different (2×2) and (11×8) surface structures of elemental Te^0 have been identified, with an approximate distance of 5.6 Å between nearest spots.[46] Therefore, the Te atoms should somehow move to modify their adsorption sites from the $(2 \times \sqrt{3})$ rectangular arrange to a (2×2) pattern and vice versa, during the redox process at 0.83 V in both oxygen- and TeO_2-free solutions.[46] In contrast, the existence of a rectangular $(2 \times \sqrt{3})$ adlayer of elemental Te has been reported in a TeO_2-saturated 0.05M H_2SO_4 solution, although the reason for these different structures in TeO_2-free and TeO_2-containing solutions is currently unknown.[48]

Following the above description, the charge under the peak at ~0.83 V can be used to characterize the tellurium coverage for $\theta_{Te} < 0.25$. Similarly, the amount of tellurium on the surface could be also quantified by measuring the blockage of the H_{ads}. From an analysis of the electric charges linked to adsorption states of the uncovered Pt(111) sites, $q^{\theta_{Te}}_{H_{ads}}$, and the redox process of Te adatoms, $q^{\theta_{Te}}_{Te_{ads}}$, a linear relationship has been measured,[1] as can be also seen in Fig. S1, with each adsorbed tellurium atom blocking four Pt(111) sites. In developing this relationship, since the Te-redox process overlaps with the adsorption of OH_{ads}, $q^{\theta_{Te}}_{Te_{ads}}$ should be approximated by subtracting from the integrated charge between 0.5 V and 0.9 V the charge attributed to OH_{ads}. The later can be calculated by assuming also a linear dependence between the degree of blockage for OH_{ads} sites and θ_{Te}. Under those assumptions, a linear relationship can be derived to approach θ_{Te} from a careful integration of the H_{ads} region on Te–Pt(111) according to the following equation:

$$q^{\theta_{Te}}_{H_{ads}} = q^{\theta_{Te}=0}_{H_{ads}}(1 - 4\theta_{Te}), \quad (3)$$

with $q^{\theta_{Te}}_{H_{ads}}$ representing the electric charge density for hydrogen adsorption at a given coverage of tellurium atoms and $q^{\theta_{Te}=0}_{H_{ads}}$ representing the electric charge density corresponding to the hydrogen adsorption on a clean Pt(111) surface. The fact that a linear relationship between $q^{\theta_{Te}}_{H_{ads}}$ vs $q^{\theta_{Te}}_{Te_{ads}}$ and $q^{\theta_{Te}}_{OH_{ads}}$ vs $q^{\theta_{Te}}_{Te_{ads}}$ is measured for $\theta_{Te} < 0.25$ suggests that adsorption of Te atoms only play a physical site blocking role, a third body effect, and it does not alter adsorption properties of H_{ads} and OH_{ads}. Otherwise, a different relationship between these electric charges densities would have been recorded.[1]

Coverages higher than $\theta_{Te} = 0.25$, giving rise to oversaturated adlayers, can be also achieved in the electrochemical environment by performing successive cycles after the maximum charge in the region ~0.83 V has been reached, which indicates a $\theta_{Te} = 0.25$. For those coverages, the CV evidences an additional sharp peak at 0.860 V, as can be seen in Fig. 1(d), and the charge under the two Te-oxidation peaks diminishes in a non-linear way with each additional cycle performed to further increase θ_{Te}, until both oxidation peaks completely disappear.[1] In this case, since the clear relation between $q^{\theta_{Te}}_{H_{ads}}$ vs $q^{\theta_{Te}}_{Te_{ads}}$ is lost, θ_{Te} cannot be easily determined, although it can be estimated from a plot of $q^{\theta_{Te}}_{Te_{ads}}$ vs the number of cycles, as explained in Ref. 1. Following this procedure, a $\theta_{Te} \sim 0.38$ has been estimated for the CV given in Fig. 1(d). On the other hand, high Te coverages lead to the appearance of surface defects on the well-ordered Pt(111) after Te desorption, indicating the damage of the Pt(111) substrate.[1]

Regarding the surface structure at high Te-coverages, STM measurements for $\theta_{Te} > 0.25$ have shown that as additional Te is deposited, the surface structure of the reduced Te–Pt(111) adlayer evolves from a rectangular $c(3 \times \sqrt{3})$ structure for $\theta_{Te} = 0.33$, with a separation between the spots of 4.7 Å, to a rectangular $c(2 \times \sqrt{3})$ for a $\theta_{Te} = 0.50$, induced by the mobility of elemental Te atoms.[48] It is proposed that the compression of the reduced adlayer at $\theta_{Te} = 0.25$ by increasing θ_{Te} results in a loss of space for accommodating oxygen atoms needed to form a stable oxygenated Te–Pt(111).[47,48] Therefore, increasing the Te coverage beyond 0.25 would progressively decrease the occurrence of the surface redox process at 0.83 V, i.e., the oxidation of the elemental Te–Pt(111) adlayer, eventually rendering the adlayer electrochemically inactive, as experimentally found.[1,47,48]

The loss in lattice space at coverages higher than 0.25 would explain the appearance of the high potential peak and the decrease in the integrated charge in this potential region in Fig. 1(d), as well as the lower adlayer stability in oxygenated solutions, described above, since adlayer oxidation is more difficult to take place. Note that, in order to accommodate the oxygen atoms required for the oxidation, a portion of the compressed domains on the reduced Te–Pt(111) adlayer should desorb. Therefore, a shift toward more positive potentials is recorded, since more energy is required for the oxygenation reaction to occur. Similarly, the lack of space for oxygen atoms decreases the extent of the oxidation process, and less charge is transferred in the redox process.

B. Oxygen reduction on Te modified Pt(111) surfaces in non-adsorbing electrolytes

Polarization curves for the oxygen reduction in 0.1M $HClO_4$ on hanging meniscus Te-modified and clean-Pt(111) rotating at $\omega = 2500$ rpm and stationary electrodes are shown in Fig. 2. On bare Pt(111), the reduction of oxygen is mainly a four-electron pathway, starting at ~1.0 V, as evidenced in Fig. 2(a).[8,33,50] The limiting current density, j_{lim}, is reached at potentials lower than 0.7 V, although at potentials lower than ~0.3 V, where the hydrogen adsorption/desorption process takes place in O_2-free solutions (see Fig. 1), two current drops appear in the CV and H_2O_2 is simultaneously detected by the ring in a rotating ring-disk setup.[8,33] The synchronized occurrence of these two processes led to initially conclude that H_{ads} would either inhibit the O–O bond scission or block surface sites required for bond cleavage.[8,33] However, recent experiments regarding the reduction of H_2O_2 at different *p*Hs have pointed toward surface charge effects, instead of H_{ads}, as the origin of these two current drops.[51]

Three main noticeable differences can be distinguished between CVs given in Fig. 2(a), where ORR polarization curves on clean and Te-modified rotating Pt(111) electrodes at high Te coverages ($\theta_{Te} \approx 0.21$) are given. First, the reaction is kinetically hindered at high potentials, evidenced by the shift toward less positive values of both the reaction onset, $E^{onset}{}_{ORR}$, and the half-wave

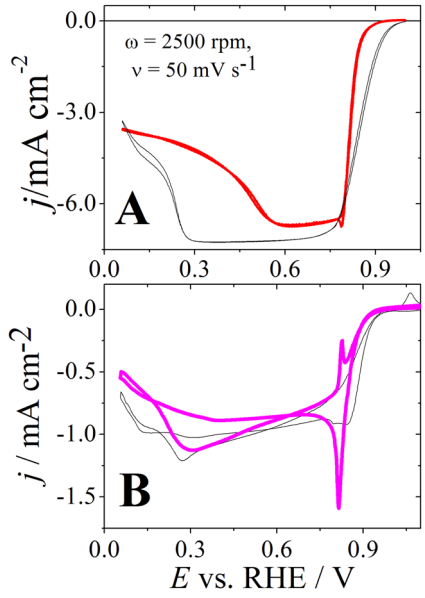

FIG. 2. Oxygen reduction on hanging meniscus at rotating disk Te–Pt(111) electrodes at 2500 rpm and $\theta_{Te} \approx 0.21$ in O_2-saturated 0.1M $HClO_4$ solutions (a) and at stationary electrodes, $\theta_{Te} \approx 0.15$ (b). Scan rate: 0.05 V s^{-1}. Polarization curve on clean Pt(111) is also given (thin line).

potential, $E^{1/2}_{ORR}$, relative to the ORR polarization curve on clean Pt(111) by ~75 mV and 30 mV, respectively. Moreover, it appears that this decrease in the ORR activity is mirrored by the appearance of oxygenated-Te species on the surface, since reduction currents quickly change from a kinetically controlled to a total mass-controlled region once the reduction of the oxygenated Te-adlayer occurs.

Second, the two current drops at $E > 0.3$ V described to occur on bare surfaces take place at more positive potentials, and third, there is a decrease in the absolute value of the limiting current density. The extent of these changes depends on the Te coverage, θ_{Te}. For data in Fig. 2(a), E^{onset}_{ORR} and $E^{1/2}_{ORR}$ shift by ~75 mV and 30 mV, respectively; the current drop after j_{lim} has been reached, starting at ~$E > 0.56$ V, and j_{lim} is ~7% lower than the value recorded in the absence of Te on the surface. In this last case, the small variation in j_{lim} in Fig. 2(a) could appear either because of differences on the electrode hanging meniscus between measurements[30,45] or due to the effect of the Te-adlayer on the electrode in ORR. The recovery of j_{lim} after the stripping of Te adatoms by continuous cycling at high potentials, while keeping the ordered surface structure, as depicted in Fig. S2, strongly supports the latter possibility. Here, it is important to mention that this decrease in j_{lim} cannot be attributed to an increase in H_2O_2 production, since there is no change in j_{lim} during the reduction of H_2O_2 in O_2-free, 0.1M $HClO_4$ under similar conditions, as evidenced in Fig. S3.

While surface charge effects may be responsible for the shift toward high potentials of the current decay after j_{lim} has been reached on Te-modified surfaces, depicted in Fig. 2(a), as discussed above, changes in the structure of the interfacial water close to the surface could account for the slight decrease in j_{lim}.[54] A gradual diminution in j_{lim} during the ORR, without an increase in H_2O_2 formation, has also been found in clean surfaces as the *p*H of the solution is increased, and it has been attributed to a kinetic effect on the reduction of OOH*.[52,55] It is expected that, since the reduction of this species would require the addition of a proton, its kinetics would be affected by the structure of water close to the surface and more difficult to achieve in neutral *p*H values, relative to acid solutions.[52,55] This topic will be discussed in more detail in a forthcoming paper.

Additionally, note that, in O_2-saturated solutions, the reduction of the oxygenated Te–Pt(111) adlayer occurs almost at ~0.79 V, a potential 35 mV less positive than the one in O_2-free solutions [see Fig. 1(c)], as clearly distinguishable in the negative-going scan in Fig. 2(a), suggesting that dissolved oxygen can stabilize the oxygenated Te adlayer. Nonetheless, despite this increase in the stability, it is worth mentioning that it is not possible to obtain long-term stable Te-adlayers with $\theta_{Te} > 0.13$–0.15 in O_2-saturated solutions, evidenced by a change in *j*–*E* profiles recorded in O_2-free solutions before and after a continuous cycling of the electrode up to $E > 0.90$ V.

A close look into the ORR polarization curve during the positive-going scan on Te–Pt(111) in Fig. 2(a) reveals that no oxidation peak for the reduced adlayer is evident, indicating that dissolved oxygen can either directly oxidize the reduced Te-adlayer or promote its oxidation by water, as indicated in Eq. (2), but in a non-electrochemical process. Otherwise, positive currents produced from the oxidation of the adlayer should have been recorded in the positive-going scan, which is not the case in the ORR curve given in Fig. 2(a). Additional support to this hypothesis is provided by the fact that at faster scan rates, *ν*, relative to the one in Fig. 2(a), the Te-oxidation peak begins to appear, as shown in Fig. S4, although a faster *ν* is required at a faster ω for an equivalent effect, evidencing not only the competence between the chemical and electrochemical oxidation of reduced Te adatoms but also an influence of ω on it. Therefore, dissolved oxygen itself may inhibit the ORR by both promoting the oxidation of adsorbed Te species and stabilizing the resulting oxygenated Te adlayer.

On the other hand, as can be understood from Fig. 2(b), the ORR on Te-modified stationary electrodes also begins at less positive potentials relative to the activity on clean Pt(111), although the magnitude of the inhibition is lower than that on rotating electrodes. For example, for the data in Fig. 2(b), E^{onset}_{ORR} shifts ~40 mV, while the negative shift in E^{onset}_{ORR} on rotating electrodes at an equivalent coverage is ~60 mV. This result evidences the existence of electronic effects between adsorbed reactive species during the reduction of dissolved oxygen and adsorbed species on the Te-adlayer, which in turns would modify adsorption properties of the surface, i.e., the apparent ΔG_{ads}^{ORR} of ORR reactive species. This electronic effect can be explained in light of the stabilizing effect of O_2 on the Te-adlayer.

In addition, in contrast to results in Fig. 2(a), characteristic peaks for the Te-redox process observed in O_2-free solutions clearly appear superimposed on ORR reduction currents, and it is possible to completely suppress this contribution by simply subtracting the CV in O_2-free solutions from ORR curves, as shown in Fig. S5. This difference between rotating and stationary electrodes in the appearance of the Te-oxidation peak during the positive-going scan at 0.05 V s^{-1} suggests that by increasing the O_2 flux close to the

surface and by rotating the electrode, the oxidation peak for the reduced Te-adlayer disappears and the stability of the oxygenated adlayer increases, since its reduction peak shifts toward less positive potentials, in agreement with what has been described above from the results at faster ν and ω.

Once the main effects of Te adatoms on the ORR have been described, in Secs. III C–III F, the discussion will focus on the analysis of the ORR inhibition at high potentials in Te–Pt(111) surfaces, in light of site blocking and/or electronic (ligand) effects. These two effects have been largely employed to explain the ORR activity and selectivity on Pt(111) electrodes in different supporting electrolytes[8] and many adatom systems,[4–7,14,15,28,35,36] and information regarding the role of surface spectator species[4,5,8,14,15,28,35,36] and the chemical environment of the electrode surface at the atomic level on the ORR kinetics has been reported.[4–7,14,35,36,41] This information is crucial for a better understanding of the molecular processes occurring during the ORR on Pt-based materials and for developing new criteria to assist the electrocatalyst design for fuel cell technology.

C. The effect of Te-coverage on the ORR at Te-Pt(111) surfaces

Similar changes in the ORR activity to the ones described above have also been reported to occur on bismuth modified Pt(100) single crystals, but in Bi-containing solutions,[14] instead of adatom-free solutions reported in this work. In this case, results were explained by considering that, besides a physical site blocking effect of Bi adatoms themselves and Bi-induced oxygenated species, adsorbed Bi would also alter the electronic properties of Pt surface atoms, which in turn would change the adsorption properties of H_{ads}, OH_{ads}, and adsorbed anions from the supporting electrolyte.

On Te-modified Pt(111) surfaces, however, a modification of the adsorption properties of H_{ads} and OH_{ads} is not expected to occur in Te–Pt(111) surfaces at $\theta_{Te} < 0.25$. This is because, as discussed in Sec. III A, a linear relationship between electric charges linked to adsorption states of uncovered Pt(111) sites, represented by the measured H_{ads} charge on the Te–Pt(111) surface, $q_{H_{ads}}^{\theta_{Te}}$, and the adsorption states covered by Te-species, calculated from the redox process of Te adatoms, $q_{Te_{ads}}^{\theta_{Te}}$, has been calculated,[1] as seen in Fig. S1. Conversely, simple site-blocking and/or negative electronic effects may be responsible for results in Fig. 2(a). In this case, it would be expected that the magnitude of the inhibition in the ORR activity will proportionally depend on the adatom's coverage. Moreover, by analyzing the changes in ORR kinetic current densities as a function of θ_{Te}, it would be possible to shed light into the chemical nature and/or atomic structure of reaction sites, which has been reported for the ORR on Ag-,[4] Cu-,[15] and Br-modified Pt(111) surfaces.[5,15,16,28]

Within this goal, the ORR on Te–Pt(111) was studied further by varying the Te-surface coverage, and some CVs evidencing changes in the ORR dynamics at rotating electrodes by increasing θ_{Te} are resumed in Fig. 3(a). Some results at stationary electrodes are also given in Fig. S5. From these figures, it is clear that increasing Te-coverages from $0 < \theta_{Te} < 0.25$ augments the kinetic ORR inhibition at high potentials, as can be clearly seen in Fig. 3(a), and the magnitude of this inhibition also depends on the O_2-flux, being more pronounced on rotating than on stationary electrodes, as discussed above. This result is better illustrated in Fig. 4, where kinetic current densities at 0.90 V and 0.85 V and kinetic current density curves as a function of θ_{Te} on Te-coated and Te-free Pt(111) electrodes are summarized.

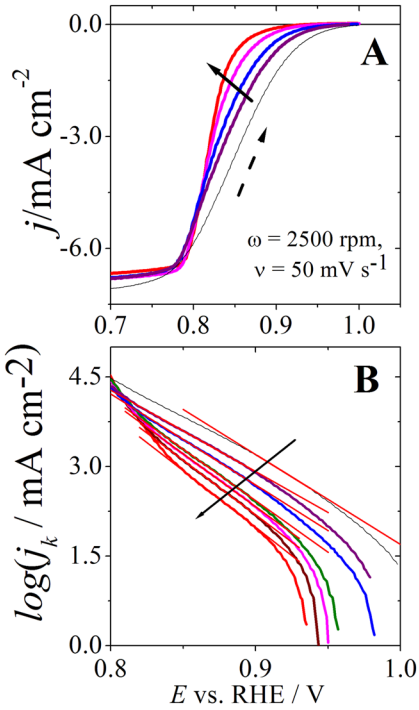

FIG. 3. Positive-going sweep for the oxygen reduction on hanging meniscus at rotating disk Te–Pt(111) electrodes in O_2-saturated 0.1M $HClO_4$ solutions at $\theta_{Te} \approx 0.08$, 0.10, 0.17, and 0.21. (a) Tafel plots at different Te-coverages, $\theta_{Te} \approx 0.08$, 0.10, 0.15, 0.17, 0.19, and 0.21. (b) Rotation rate: 2500 rpm. Scan rate: 0.05 V s^{-1}. Polarization curve on clean Pt(111) is also given (thin line). Solid arrows indicate the increase in θ_{Te}, while the dashed arrow in Fig. 3(a) indicates the direction of the sweep.

Kinetic analysis of curves in Fig. 3(a) were performed by employing the Koutecky–Levich equation,[8,27,30,33,45,50,52] and results in the form of Tafel plots are shown in Fig. 3(b). From these curves, Tafel slopes between −53 mV and −62 mV at decreasing θ_{Te} from 0.21 to 0.08 were approximated, implying that they are not significantly affected by θ_{Te}. Moreover, since for bare Pt(111), a Tafel slope of −66 mV at potentials close to $E^{onset}{}_{ORR}$ is estimated, in agreement with the reported values,[8,27,30,33,45,50,52] it appears that the rate determining step (RDS) in the ORR mechanism is the same in all surfaces. Furthermore, considering that 3.8 and 3.6 electrons are transferred during the ORR on Te-clean and Te-modified Pt(111) electrodes, respectively, calculated by employing Levich's equation,[8,27,30,33,45,50,52] it is inferred that the reaction is predominantly a $4e^-$ reduction to H_2O. Therefore, although adsorbed Te atoms negatively shift $E^{onset}{}_{ORR}$ and $E^{1/2}{}_{ORR}$, it seems that the whole reaction mechanism from $E^{onset}{}_{ORR}$ to $E < 0.56$ V, where j_{lim} are measured, is not significantly modified.

Tafel slopes lower than −118 mV on Pt surfaces have been commonly interpreted as a consequence of Temkin adsorption

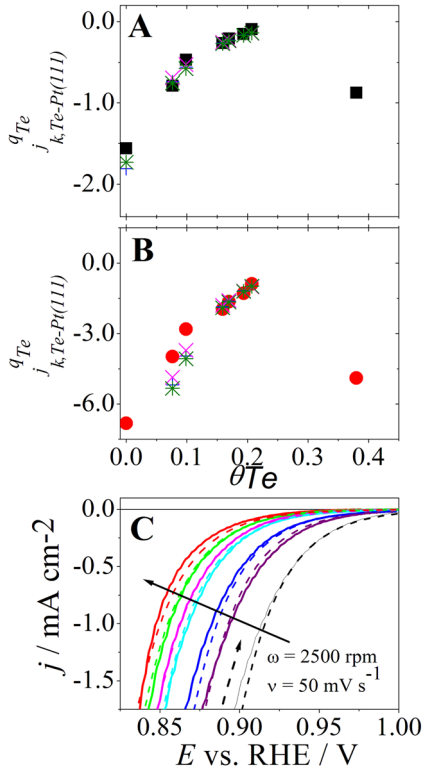

FIG. 4. Experimental and simulated ORR activity on hanging meniscus Te–Pt(111) in O_2-saturated 0.1M $HClO_4$ solutions. (a) j_k at 0.90 (black squares) and (b) at 0.85 V (red circle) as a function of θ_{Te}. Simulated kinetic current densities are calculated by considering site-blocking effects (model 1) [$(1-\theta_{Te})^{11}$, green stars] and electronic effects (model 2) [$\exp(-\gamma r_{Te,ads}\theta_{Te}/RT)$ with $r_{Te,ads}/RT$ = 24, pink cross]. Both effects are considered in model 3 (blue plus) and model parameters are site-blocking $(1-\theta_{Te})^7$ and electronic effects, $r_{Te,ads}/RT$ = 9. In the last case, full simulated kinetic current densities (dashed line), besides experimental curves, are given in (c). See text for details. In Fig. 4(c), dashed and solid arrows indicate the direction of the sweep and the increase in θ_{Te}, respectively.

conditions for ORR intermediates.[8,33,50] Thus, comparable Tafel slopes on Te-modified and Te-free Pt(111) electrodes would, in principle, suggest that the apparent standard adsorption Gibbs energy of reactive species, ΔG_{ads}^{ORR}, such as molecular O_2 or adsorbed intermediates, is not significantly modified by neighboring oxidized Te adatoms.[28] However, considering that on Te–Pt(111), adsorption of OH_{ads} is largely blocked, Temkin adsorption conditions between OH_{ads} and ORR reactive species do not appear feasible to occur. Moreover, since the magnitude of the ORR inhibition depends on O_2-flux, as discussed above, it would be rather improbable that average energetic interactions between oxidized Te and ORR reactive species would be similar to the ones between OH_{ads} and ORR reactive species, which would also explain the resemblance between Tafel slopes. Therefore, it is possible that the similar Tafel slopes appear because of the existence of a chemical step following the first electron transfer as the RDS in the mechanism, as recently suggested from transient experiments and digital simulations of ORR polarization curves on (Poly)Pt.[53]

On the other hand, it is important to note that no ORR reduction peak at 0.85 V is displayed on stationary Te–Pt(111) surfaces in Fig. 2(b), as in the case of bare Pt(111). This fact holds true even at low Te-coverages $\theta_{Te} \approx 0.05$ or after holding the potential by several minutes at 0.9 < E < 1.15 V, a procedure that has been reported to increase the magnitude of the ORR peak at 0.85 V on both Pt(111) and (poly)Pt stationary electrodes.[50,56] Thus, it would be possible that, instead of a simple site-blocking effect, a part of ORR reduction currents comes from a catalysis of the ORR by the redox cycle of Te adatoms on the surface, as suggested to occur in the case of Tl adlayers on Au(111) electrodes.[35,36] In this case, the decrease in the ORR activity at high potentials at increasing θ_{Te}, as evidenced in Figs. 4(a) and 4(b), would appear because the oxidation of reduced Te-adlayers slightly shifts toward higher potentials by increasing θ_{Te}, as seen in Fig. 1 and described in Sec. III A.

In this framework, dissolved oxygen would chemically oxidize the reduced Te-adlayer, and reduction currents would appear because of the subsequent reduction of this oxygenated Te-adlayer. At stationary electrodes, the redox cycle of Te-adatoms would be fast enough to sustain the reaction with dissolved oxygen and water from the electrolyte, as indicated in Eq. (2). However, once the O_2-flux is increased by rotating the electrode, the chemical oxidation of the reduced Te-adlayer by O_2 would become faster than the electrochemical oxidation, and the corresponding oxidation peak for this last process would disappear from the CV. The stronger inhibition on the ORR at rotating, relative to stationary, electrodes would be a consequence of the increased stability of the oxygenated Te-adlayer at high O_2-flux.

D. Modeling of the ORR on Te–Pt(111) surfaces: Surface site availability vs electronic effects

From the discussion above, it is clear that on Te–Pt(111) surfaces, the ORR is kinetically inhibited at high potentials and the magnitude of this inhibition depends on the Te-coverage, $0 < \theta_{Te} < 0.25$, and the O_2-flux close to the surface. Besides, it appears that the stability of the Te–Pt(111) adlayer increases in the presence of oxygen, although in this case, long-term stable Te adlayers with $\theta_{Te} > 0.13$–0.15 cannot be prepared. However, at this point, the exact process responsible for the ORR inhibition is not clear, since both site-blocking and electronic effects may be operative during the reduction, together with the possibility of a potential ORR catalysis by the redox state of Te adatoms.

As an attempt to shed light to those questions raised above, ORR kinetic current densities as a function of θ_{Te} were simulated by considering the occurrence of either site-blocking or electronic effects alone and also by including these two effects into a simple mean field model. It is expected that this model would allow for a more quantitative picture and understanding of results displayed in Figs. 2 and 3. Considering the past studies about the ORR on Pt-based surfaces, the following expression was employed to simulate the ORR reaction rate:[8,28,32,42]

$$j = nFkc_{O_2}(1-\theta_{ads})^x \exp(-\beta n' F(E-E^0)/RT)\exp(-\gamma r_{ads}\theta_{ads}/RT), \quad (4)$$

where j is the kinetic current density, F (96 485.3 C mol^{-1}), R (8.314 J K^{-1} mol^{-1}), T (298.15 K), and E^0 (1.229 V) have their

usual meaning, n represents the total number of electrons transferred in reaction (4), n' represents the number of electrons transferred in the RDS, k is the rate constant of the RDS, c_{O_2} is the concentration of O_2 in the solution (0.001 26 mol l^{-1}), θ_{ads} is the coverage of blocking species, x is the number of surface sites blocked by the adsorbate and thus excluded for the ORR to occur,[4] β and γ are symmetry factors (assumed to be 0.5), E is the applied potential, and $r_{ads}\theta_{ads}$ represents the change in ΔG_{ads}^{ORR} with the adsorbates' coverage. The ratio r_{ads}/RT is commonly called the Frumkin interaction factor.

In developing Eq. (4),[8,30,33,42,45,50,57] it has been implicitly assumed that the ORR is first order regarding the concentration of oxygen, as widely recognized for Pt surfaces. According to this expression, the ORR reaction rate on adatom-modified electrodes can be affected by changes in either the pre-exponential term through the term $(1 - \theta_{ads})^x$, which would describe site-blocking effects of adsorbed species, or the second exponential term $\exp(-\gamma r_{ads}\theta_{ads}/RT)$, which would account for coverage-dependent electronic effects of adsorbates on the ORR kinetics, or both. The first expression has been derived by using a simple statistical approach for describing the reaction inhibition by one adsorbed adatom blocking x surface sites for the reaction and calculating the probability of occurrence of having such a structure on the surface.[4] The second term appears by including electronic effects as a linear variation of ΔG_{ads}^{ORR} with θ_{ads}, and it can be interpreted as a potential shift of ORR kinetic currents toward negative (positive) potentials when an inhibiting (promoting) effect is expected.[32]

Additionally, since the main goal of the proposed model is to describe the ORR inhibition by adsorbed Te relative to the activity of Pt(111), three other assumptions were made before the mathematical fitting of experimental data to Eq. (4); (i) To avoid any mechanistic assumption regarding the nature of the RDS from the measured Tafel slope on Pt(111), i.e., either a first charge transfer step under Temkin adsorption conditions or a chemical step following the first charge transfer, as discussed above. The term $-\beta n' F/RT$ was considered to be 59 mV, i.e., the predicted theoretical value by employing an integer number (2) to give a Tafel slope close to the experimental value (66 mV); (ii) a negligible coverage of ORR reactive intermediates, as is usually reported for the ORR on Pt surfaces.[8,42,56,57] (iii) Also, x and r_{ads} are independent of θ_{Te}, although they depend on the O_2-flux.

Therefore, model variables are k, x, and/or r_{ads}. Contrarily, θ_{ads}, in our case considered equal to θ_{Te}, can be regarded as a constant parameter, rather than a system variable, since ORR curves in Figs. 2 and 3 were taken based on experiments in adatom-free solutions, and thus, θ_{Te} is constant during measurements. To assure this last condition, j–E profiles in O_2-free solutions were always collected before and after each measurement of ORR polarization curves. Inside this framework, note that Eq. (4) holds true only for electrode potentials for which normalized ORR kinetic current densities on Te–Pt(111) relative to Pt(111), $j_{k,TePt(111)}^{\theta_{Te}}(E)/j_{k,Pt(111)}(E)$, at a given θ_{Te}, superimpose.[4] Figure 5 resumes a plot of $j_{k,TePt(111)}^{\theta_{Te}}(E)/j_{k,Pt(111)}(E)$ as a function of θ_{Te} at different potentials.

From Fig. 5, it is seen that experimental data, in both scan directions, only fit into a model described by Eq. (4) at potentials close to the reaction onset, $0.875 < E < 0.955$ V, i.e., only at those potentials

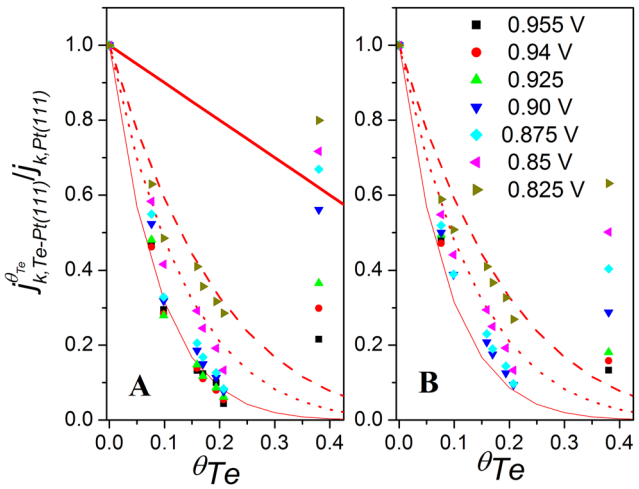

FIG. 5. Normalized O_2 reduction current on a rotating Te–Pt(111) electrode as a function of Te coverage at different potentials (points) during the positive- (a) and negative-going scans (b). Calculated curves for $(1 - \theta_{Te})^1$ (solid line), $(1 - \theta_{Te})^5$ (dashed line), $(1 - \theta_{Te})^7$ (dotted line), and $(1 - \theta_{Te})^{11}$ (thin line) dependences. See text for details.

the ratio $j_{k,TePt(111)}^{\theta_{Te}}(E)/j_{k,Pt(111)}(E)$ is almost constant at a fixed θ_{Te}, especially at high coverages. Deviations of experimental data from the model described by Eq. (4) at lower potentials are likely to occur because of both the reduction of the oxygenated Te-adlayer and the desorption of OH_{ads}, two processes not accounted by the model. Moreover, at $E < 0.875$ V, the ratio $j_{k,TePt(111)}^{\theta_{Te}}(E)/j_{k,Pt(111)}(E)$ continuously increases as E decreases, indicating that the reactivity of the Te–Pt(111) surfaces is increasing, relative to the ORR activity of Pt(111). This fact strongly suggests that Eq. (4) would be only valid for describing the ORR on oxygenated Te–Pt(111) adlayers, and thus, these species are the ones responsible for ORR inhibition at high potentials.

As mentioned above, three different systems were analyzed in this work. In the first model, model 1, experimental data were fitted by only considering k and x as system variables in order to evaluate simple site-blocking effects of Te adatoms. Correspondingly, the second model, model 2, only considers k and r_{ads} to solely represent electronic effects of Te adatoms on the ORR kinetics. Finally, the third model, model 3, describes the situation where both site-blocking and electronic effects are operative, and in this case, three variables need to be determined, k, x, and r_{ads}. In the last case, since only one independent system parameter can be determined from experimental data, i.e., x or r_{ads}, it was arbitrarily assumed that Te adsorbs on threefold symmetry hollow sites, as considered in previous STM studies,[46] and it presents the highest site-blocking inhibition effect, i.e., $x = 7$.[4] Nevertheless, as will be discussed below, the quality of the fitting does not significantly depend on the exact value.

Simulated kinetic current densities at 0.90 V and 0.85 V on Te-coated and Te-free Pt(111) electrodes, calculated by employing $x = 11$ (model 1), $r_{Te,ads}/RT = 24$ (model 2), and $x = 7$ and

$r_{Te,ads}/RT$ = 9 (model 3), are given in Figs. 4(a) and 4(b), respectively. Full kinetic current densities curves for model 3 are given in Fig. 4(c) while for models 1 and 2 are resumed in Fig. S6. Additionally, expected theoretical $j^{\theta_{Te}}_{k,TePt(111)}(E)/j_{k,Pt(111)}(E)$ curves at different θ_{Te}, calculated by considering only site blocking effects, with x = 1, 5, 7, and 11, i.e., $(1-\theta_{Te})^1$, $(1-\theta_{Te})^5$, $(1-\theta_{Te})^7$, and $(1-\theta_{Te})^{11}$, are also given in Fig. 5. It is seen that in this case, the curve for $(1-\theta_{Te})^{11}$ follows quite well the experimental data during the positive-going sweep up to ~E = 0.875 V, especially at high θ_{Te}.

For each model, x (model 1) or r_{ads} (models 2 and 3) were determined from the slope of a plot of either log(j) vs log$(1-\theta_{Te})$ or log(j) vs θ_{Te}, respectively,[4] by employing only data at electrode potentials where $j^{\theta_{Te}}_{k,TePt(111)}(E)/j_{k,Pt(111)}(E)$ superimpose, as indicated in Fig. 5. In addition, a value of $k = 1.05\times10^{-11}$ cm s^{-1}, equivalent to $j_0 = 5.1\times10^{-3}$ μA cm^{-2}, estimated from fitting Eq. (4) to experimental ORR kinetic current densities on clean Pt(111) at high potentials, is employed to simulate all curves in Fig. 4(c) and Fig. S6. In a previous study, a value of $j_0 = 1.9\times10^{-3}$ μA cm^{-2} was reported, calculated from experimental data by assuming a Tafel slope of 59 mV at high potentials.[32]

As can be understood from Fig. 4(c) and Fig. S6, all three models give similar fitting to experimental curves, and therefore, from these data, it is not possible to conclude about the exact nature of the process responsible for the ORR inhibition on Te–Pt(111) surfaces. In this sense, simulations demonstrate that it is not possible to discriminate between site blocking and electronic effects by simply fitting experimental data to mean field models, Eq. (4), and also likely to more complex atomistic models that would explicitly include surface structure effects,[37] such as those based on Monte Carlo simulations.

On the other hand, note that for fitting model 1, an extremely large value for the number of surface sites blocked by the adsorbate has been estimated, i.e., x = 11. This value is almost an unrealistic one, since a careful analysis of probable site-exclusion by adatoms on (111) surfaces revealed that the highest possible inhibition effect occurs for x = 7, determined to occur when both the adatom and the reacting species adsorb on hollow sites.[4] Thus, the higher value calculated by fitting experimental data to model 1, i.e., 11 > 7, may indicate that site-blocking effects alone cannot account for the reaction inhibition by oxygenated Te adatoms illustrated in Figs. 2 and 3. Therefore, either electronic effects alone (model 2) or both electronic and site-blocking effects (model 3) should be responsible for the ORR inhibition.

Nevertheless, simulations of model 2 and 3 do not allow us to differentiate between the occurrence of electronic effects alone and both electronic and site-blocking effects. In the last situation, for example, there is no significant improvement in the data fitting if, instead of employing x = 7 as represented in Fig. 4, a lower value of x is employed. In this case, the value of $r_{Te,ads}/RT$ will increase to account for the effect of a lower x, and a similar mathematical fitting is calculated for all curves. $r_{Te,ads}/RT$ reaches a maximum value when x = 0, as in model 2, i.e., $r_{Te,ads}/RT$ = 24. A Frumkin interaction factor of 41.2 has been reported for the repulsive interaction between neighboring O_{ads} adatoms on Pt(111),[58] and thus, pure electronic effects between oxygenated Te adatoms and ORR intermediates could perfectly account for ORR inhibition at high potentials reported in this work.

E. ORR on oversaturated Te–Pt(111) surfaces: The role of reduced Te–Pt(111) adlayers

By comparing simulations of Eq. (4) and experimental data, it was possible to clearly identify the oxygenated Te-adlayer as the poisoning species of the ORR at high potentials by either an electronic effect alone or a combination of electronic and site-blocking effects. However, it was not possible to conclude about the role of the reduced Te-adlayer, since no reduced Te adatoms remain on the surface once the redox process of the adlayer occurs, as long as $\theta_{Te} < 0.25$. Nonetheless, at oversaturated adlayers (i.e., $\theta_{Te} > 0.25$), CVs in O_2-free solutions indicate that the ratio between oxygenated and reduced Te adatoms becomes lower than 1, i.e., the coverage of oxygenated atoms after the redox process at ~0.83 V takes place (see Fig. 1) is now lower than θ_{Te}. Hence, by evaluating the ORR on oversaturated Te-adlayers, it may be possible to assess the role of reduced Te adatoms on the ORR.

If reduced Te adatoms poison the ORR, a larger ORR inhibition than the one expected from the coverage of oxygenated adatoms should be measured on oversaturated Te–Pt(111) surfaces. Similarly, if the redox properties of Te adatoms catalyze the ORR, it would be expected that a decrease in these redox properties, as it occurs in oversaturated adlayers, would also decrease ORR reduction currents. Figure 6 summarizes the ORR on an oversaturated Te–Pt(111) adlayer, θ_{Te} = 0.38. This Te-coverage was selected because it is not high enough to destroy the ordered Pt(111) substrate structure, as verified by the absence of surface defects on the j–E profile once the Te adatoms have been removed from the surface by continuous cycling up to E < 1.1 V. For this adlayer, a coverage of oxygenated Te adatoms, $\theta_{TeOx} \approx 0.12$, has been estimated from the charge transferred in the redox process in O_2-free solutions of this layer, as shown in Fig. 1(d).

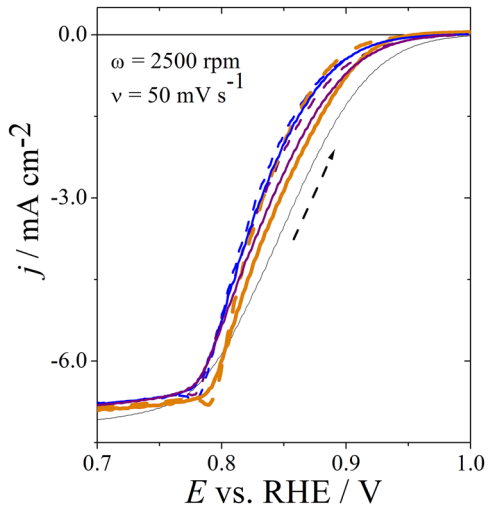

FIG. 6. Positive (solid line) and negative (dashed line) going sweeps for the oxygen reduction on the hanging meniscus rotating disk Te–Pt(111) electrode at $\theta_{Te} \approx 0.38$ in O_2-saturated 0.1M $HClO_4$. Polarization curves with $\theta_{Te} \approx 0.08$ and $\theta_{Te} \approx 0.10$ (thin line) and on clean Pt(111) are also given (thinnest line). Rotation rate: 2500 rpm. Scan rate: 0.05 V s^{-1}. Dashed arrow indicates the direction of the sweep.

From results in Fig. 6, it appears that reduced Te adatoms have neither an inhibiting/promoting effect on the ORR kinetics, despite the strong site-blocking effect on H_{ads} and OH_{ads} adsorption, seen in Fig. 1. Hence, it appears that adsorption sites for these last two species are different to the ones required for the ORR RDS to occur on Pt(111), although those sites still could be active sites for other particular intermediates participating in non-controlling steps in the ORR mechanism. This is because the oversaturated Te–Pt(111) adlayer with $\theta_{TeOx} \approx 0.12$, with virtually no adsorbed H_{ads} and OH_{ads} [see Fig. 1(d)], is slightly more active for the ORR, as shown in Fig. 6, than Te–Pt(111) adlayers with lower coverages of θ_{TeOx}, e.g., $\theta_{Te} \approx 0.08$, and measurable coverages of H_{ads} and OH_{ads} [see Fig. 1(a)]. This fact evidences that in those oversaturated adlayers, the inhibiting effect of θ_{TeOx} is counterbalanced by the excess of Te adatoms on the surface relative to the saturated layer, $\theta_{Te} = 0.25$.

Moreover, from an observation of Fig. 5, it is realized that current densities at $E < 0.9$ (0.825) V during the positive (negative) going sweep on the oversaturated Te-adlayer are even higher than the ones calculated by employing model 1 with $x = 1$, representing the lowest inhibiting effect, i.e., when each Te adatom can block only one active site for the ORR. In contrast to what has been reported for other adatoms on Pt(111) at equivalent surface coverages and structures, such as for a $(\sqrt{3} \times \sqrt{3})R30°$Me at $\theta_{Me} \approx 0.33$ of Ag,[4] Br,[16,28] or Cu,[15] an almost complete ORR inhibition has been reported. These results strongly indicate that reduced Te adatoms do not physically block active sites where the RDS of the ORR occurs.

It is possible that the small increase in the ORR activity on oversaturated Te adlayers relative to the one on Te–Pt(111) at lower coverages, seen in Fig. 6, may be the result of a restructuration of the adlayer for accommodating the additional Te adatoms, which eventually could leave patches with more diluted, or even clean, Pt(111) atoms on the surface. Alternatively, it is also possible that the ORR on the reduced Te-adlayer takes place as it happens on bare Pt(111) surfaces and, if this is the case, increased ORR activity on oversaturated Te–Pt(111) adlayers would appear because of an increase in the surface site availability, i.e., the increase in the amount of reduced Te adatoms. Unfortunately, results from this work do not allow us to discriminate between these two hypotheses.

F. ORR on Te–Pt(111) in specifically adsorbing electrolytes

It is been widely accepted that in strongly adsorbing electrolytes, the ORR catalytic activity of Pt single crystals markedly depends on the electrode's crystallographic orientation and the symmetry of the adsorbing anion relative to the structure of the surface.[32,34,40] For Pt(111), it has been shown that anions adsorbed onto threefold sites, such as phosphate and sulfate anions, significantly shift the reaction onset toward less positive potentials, and the magnitude of this inhibition depends on the strength of the anions' adsorption, i.e., $ClO_4^- < SO_4^{2-} < H_2PO_4^-$.[8,9,27,32] In contrast, the analysis described above suggests that on Te–Pt(111), the nature of the adsorption site is less important than the oxidation state of the adlayer, since it appears that reduced Te adatoms, adsorbed also on threefold sites, do not affect the reaction, despite the strong interaction between Te atoms and the Pt(111) surface. Thus, it would be interesting to evaluate the ORR activity of Te–Pt(111) not only in non-adsorbing electrolytes but also in the presence of specifically adsorbing electrolytes, such as sulfate.[59]

Within this goal, Fig. 7 shows the voltammetry profiles of Te–Pt(111) at $\theta_{Te} \approx 0.22$ in 0.05M H_2SO_4 in Ar- and O_2-saturated solutions (2500 rpm). In this case, the Te-coverage was controlled by first adsorbing higher Te amounts and later by cycling the electrode in 0.1M $HClO_4$ at high potentials until the desired coverage was reached while keeping the well-ordered structure of the electrode. For the sake of comparison, curves on bare Pt(111) and in 0.1M $HClO_4$ on the Te–Pt(111) surface are also given. As can be understood from this figure, in the case of H_2SO_4 containing solutions, adsorption of Te adatoms enhances the electrode catalytic activity, shifting $E^{1/2}{}_{ORR}$ by more than 120 mV toward positive potentials, regarding the ORR activity on clean Pt(111) in 0.05M H_2SO_4 solutions.

A similar increase in the ORR activity in solutions containing strong adsorbing tetrahedral oxyanions has also been reported to occur by irreversibly adsorbing on Pt(111) either cyanide at an optimal coverage on phosphate and sulfate containing electrolytes[6,26] or polyvinylpyrrolidone (PVP) in H_2SO_4 solutions.[7] In both cases, results were explained to occur as a consequence of the suppression of oxyanions' adsorption via a steric, site-blocking (ensemble) mechanism.[6,7,26] However, by comparing ORR polarization curves in 0.1M $HClO_4$ and 0.05M H_2SO_4 in Fig. 7, it is realized that $SO_{4,ads}$ not only has a site-blocking effect but also a strong negative electronic effect. This is because in both solutions, the reaction practically starts at the same potential, and curves in both electrolytes

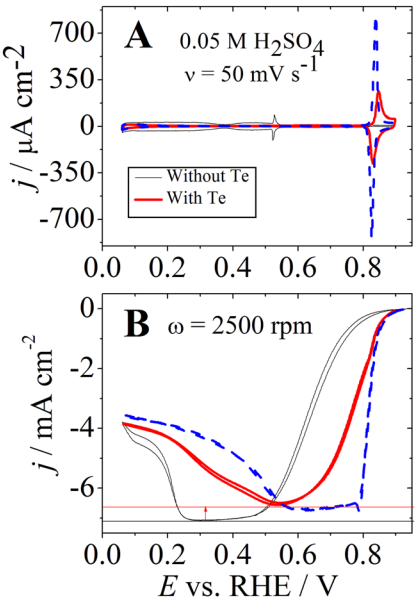

FIG. 7. Electrochemical response of Te–Pt(111) at $\theta_{Te} \approx 0.22$ in 0.05M H_2SO_4. Voltammetric profile in Ar-saturated (a) and O_2-saturated solutions (b). Data with a hanging meniscus rotating disk are taken at 2500 rpm. Voltammetric curves in $HClO_4$ at a similar Te-coverage (dashed) and on bare Pt(111) (thin line) are also given. Scan rate: 0.05 V s^{-1}.

superimpose from $E^{onset}{}_{ORR}$ until a potential where the reduction of oxygenated Te adatoms in 0.05M H_2SO_4 occurs. Once this potentials is reached, a further decrease in E gives rise to a lower ORR activity in H_2SO_4 than the one in $HClO_4$, possibly because of a small amount of co-adsorbed $SO_{4,ads}$ on the surface, indicating the strong negative electronic effect of $SO_{4,ads}$ on the ORR kinetics.

Although no clear oxidation/reduction peaks are recorded in the 0.05M H_2SO_4 solution, the reduction of the oxygenated adlayer is evidenced by the inflection point seen in the ORR polarization curve ~0.832 V, the same potential where the reduction of the oxygenated Te-adlayer takes place in O_2-free electrolytes. This is a different result than the one in Fig. 2, where the reduction peak of the Te adlayer is shifted toward less positive potentials in O_2 saturated $HClO_4$ solutions. This fact suggests a possible competitive adsorption/desorption mechanism in 0.05M H_2SO_4 in which adsorbed sulfate is displaced by Te-oxygenated species formed in the redox process of the reduced Te-adlayer. At $E < 0.832$ V, once the oxygenated adlayer is reduced, SO_{4ads} co-adsorbs on the surface, jointly with reduced Te adatoms, and the ORR becomes slower than that in $HClO_4$ solutions. The lack of a potential shift toward less positive potentials for the reduction of the oxygenated Te-adlayer in Fig. 7 indicates that in H_2SO_4-containing solutions, dissolved oxygen cannot stabilize the oxygenated Te-adlayer, possibly because of the stronger adsorption of SO_{4ads} at those potentials.

It is interesting to highlight that, despite the strongest adsorption of Te adatoms on Pt(111) relative to SO_{4ads}, the ORR on Te–Pt(111) in 0.1M $HClO_4$ is significantly faster that than on bare Pt(111) in 0.05M H_2SO_4. Nevertheless, Te adatoms inhibit sulfate adsorption, as can be seen in Fig. 7(a) from the decrease in the SO_{4ads} coverage, while keeping the 1:2 ratio proportional to the H_{ads} coverage when the Te-adlayer is prepared by desorbing Te atoms from a slightly oversaturated adlayer. Moreover, Te adatoms do not simply block SO_{4ads} adsorption sites, as in the case of H_{ads} and OH_{ads}, but also modify the SO_{4ads} adsorption energy (electronic effect), evidenced by the shift toward positive potentials of the sulfate adsorption.

Results highlighted in the previous paragraph suggest that it is the chemical nature of the adsorbing anion and not its adsorption strength that defines the catalytic role on the ORR kinetics, i.e., it appears that oxyanions/oxycations are poisoning species for the reaction, since oxygenated Te adatoms also inhibit the ORR kinetics. It is possible that, contrary to what is commonly accepted, the lack of a negative electronic effect on the OH_{ads} adsorption is what gives rise to the smaller poisoning effect of oxygenated Te adatoms on the ORR kinetics, relative to the case of bare surfaces in H_2SO_4 solutions, where a strong inhibition on the OH_{ads} adsorption is observed.

IV. CONCLUSIONS

The ORR has been studied on Te-modified Pt(111) surfaces at different coverages. At $0 < \theta_{Te} < 0.25$, adsorption of Te adatoms on Pt(111) surface kinetically hinders the ORR at high potentials, shifting the reaction onset and the half-wave potential by 75 mV and 30 mV, respectively, when $\theta_{Te} \approx 0.21$, together with a small decrease in the limiting current density and a shift toward positive potentials of the two current decays after j_{lim} has been reached.

By the analysis of experimental data in light of a simple mean field model, commonly employed to describe site-blocking and electronic effects, it is realized that oxygenated Te adatoms behave as poisoning species for the ORR. However, from electrochemical data alone, it is not possible to undoubtedly conclude about the exact nature of the process responsible for the reaction inhibition, since both site-blocking effects and electronic effects alone could account for the measured electrochemical response. However, considering the strong interaction of Te adatoms and Pt(111) surface and the highest possible inhibition effect on (111) surfaces, calculated from a careful analysis of possible site-exclusion by adatoms, either electronic effects alone or both site-blocking and electronic effects play an important role in the reaction inhibition.

Analysis of the ORR on oversaturated Te–Pt(111), $\theta_{Te} > 0.25$, adlayers suggests that the reduced Te–Pt(111) adlayer neither catalyzes nor inhibits the ORR, despite the noticeable site-blocking effect on H_{ads} and OH_{ads} adsorption. Hence, it appears that adsorption sites for these two species are different to the ones required for the ORR rate determining step to occur on Pt(111), although they still could be active sites for other non-controlling steps in the ORR mechanism.

On the other hand, the analysis of the ORR on Te–Pt(111) in 0.05M H_2SO_4 electrolytes evidenced a higher ORR activity than that on bare electrodes. These effects can be understood by considering a competitive adsorption/desorption mechanism between Te and SO_{4ads} adatoms. From the change in the CV after the adsorption of Te adatoms in oxygen-free solutions, it is seen that the coverage of specifically adsorbed sulfate ions is markedly reduced by the preferential adsorption of Te adatoms, giving rise to a pseudo-promoting catalytic effect. Nevertheless, similar to clean Pt(111), the ORR activity on Te–Pt(111) electrodes in H_2SO_4 solutions is still lower than the one registered in $HClO_4$, at similar θ_{Te}, since at the studied coverage, $\theta_{Te} \approx 0.21$, there is still a small amount of co-adsorbed sulfate on the surface, indicating the strong negative electronic effect of $SO_{4,ads}$ on the ORR kinetics.

SUPPLEMENTARY MATERIAL

See the supplementary material for the linear relation between the electric charge densities due to hydrogen adsorption and surface tellurium oxidation, additional cyclic voltammograms in stationary and rotating electrodes either in O_2-saturated or in O_2-free, H_2O_2 containing solutions, and simulated kinetic current densities by considering either site-blocking effects (model 1, $x = 11$) or electronic effects alone (model 2, $r_{Te,ads}/RT = 24$).

ACKNOWLEDGMENTS

The authors would like to thank Fundação de Amparo a Pesquisa do Estado de São Paulo (FAPESP—Proc. 2019/04484-9), Brazil (A.M.G.-M.), and the Spanish MINECO through Project No. CTQ2016-76221-P (FEDER) (J.M.F.) for financial support.

REFERENCES

[1] J. M. Feliu, M. J. Llorca, R. Gómez, and A. Aldaz, Surf. Sci. **297**, 209 (1993).
[2] E. Herrero, V. Climent, and J. M. Feliu, Electrochem. Commun. **2**, 636 (2000).
[3] R. R. Adžić and A. R. Despic, Z. Phys. Chem. **98**, 95 (1975).
[4] R. R. Adžić and J. X. Wang, J. Phys. Chem. **102**, 8988 (1998).

[5]J. X. Wang, N. S. Marinković, and R. R. Adžić, Colloids Surf., A **134**, 165 (1998).
[6]E. G. Ciapina, P. P. Lopes, R. Subbaraman, E. A. Ticianelli, V. Stamenkovic, D. Strmcnik, and N. M. Markovic, Electrochem. Commun. **60**, 30 (2015).
[7]J.-Y. Ye, G. A. Attard, A. Brew, Z.-Y. Zhou, S.-G. Sun, D. J. Morgan, and D. J. Willock, J. Phys. Chem. C **120**, 7532 (2016).
[8]N. M. Markovic and P. N. Ross, Jr., Surf. Sci. Rep. **54**, 117 (2002).
[9]A. M. Gómez-Marín and J. M. Feliu, "Oxygen reduction on platinum single crystal electrodes," in *Encyclopedia of Interfacial Chemistry: Surface Science and Electrochemistry* (Elsevier, 2018), pp. 820–830.
[10]J. Clavilier, J. M. Feliu, and A. Aldaz, J. Electroanal. Chem. **243**, 419 (1988).
[11]J. M. Feliu, A. Fernandez-Vega, A. Aldaz, and J. Clavilier, J. Electroanal. Chem. **256**, 149 (1988).
[12]J. M. Feliu, R. Gómez, M. J. Llorca, and A. Aldaz, Surf. Sci. **289**, 152 (1993).
[13]C. A. Lucas, N. M. Marković, and P. N. Ross, Phys. Rev. B **56**, 3651 (1997).
[14]T. J. Schmidt, V. R. Stamenkovic, C. A. Lucas, N. M. Markovic, and P. N. Ross, Jr., Phys. Chem. Chem. Phys. **3**, 3879 (2001).
[15]T. Abe, G. M. Swain, K. Sashikata, and K. Itaya, J. Electroanal. Chem. **382**, 73 (1995).
[16]V. Briega-Martos, G. A. B. Mello, R. M. Arán-Ais, V. Climent, E. Herrero, and J. M. Feliu, J. Electrochem. Soc. **165**, J3045 (2018).
[17]E. Herrero, A. Rodes, J. M. Pérez, J. M. Feliu, and A. Aldaz, J. Electroanal. Chem. **412**, 165 (1996).
[18]C. Lamy, J. M. Leger, J. Clavilier, and R. Parsons, J. Electroanal. Chem. **150**, 71 (1983).
[19]M. Shibata, O. Takahashi, and S. Motoo, J. Electroanal. Chem. **249**, 253 (1988).
[20]J. V. Perales-Rondón, C. Busó-Rogero, J. Solla-Gullón, E. Herrero, and J. M. Feliu, J. Electroanal. Chem. **800**, 82 (2017).
[21]M. Shibata, N. Furuya, and M. Watanabe, J. Electroanal. Chem. **267**, 163 (1989).
[22]E. Herrero, M. J. Llorca, J. M. Feliu, and A. Aldaz, J. Electroanal. Chem. **394**, 161 (1995).
[23]M. Shibata and S. Motoo, J. Electroanal. Chem. **209**, 151 (1986).
[24]M. Shibata and S. Matoo, J. Electroanal. Chem. **229**, 385 (1987).
[25]V. del Colle, J. Souza-Garcia, G. Tremiliosi-Filho, E. Herrero, and J. M. Feliu, Phys. Chem. Chem. Phys. **13**, 12163 (2011).
[26]D. Strmcnik, M. Escudero-Escribano, K. Kodama, V. R. Stamenkovic, A. Cuesta, and N. M. Marković, Nat. Chem. **2**, 880 (2010).
[27]F. El Kadiri, R. Faure, and R. Durand, J. Electroanal. Chem. **301**, 177 (1991).
[28]N. M. Marković, H. A. Gasteiger, B. N. Grgur, and P. N. Ross, J. Electroanal. Chem. **467**, 157 (1999).
[29]K. Jüttner and W. J. Lorenz, Z. Phys. Chem. **122**, 163 (1980).
[30]M. D. Maciá, J. M. Campiña, E. Herrero, and J. M. Feliu, J. Electroanal. Chem. **564**, 141 (2004).
[31]N. M. Marković, H. A. Gasteiger, and N. P. Ross, J. Phys. Chem. B **100**, 6715 (1996).
[32]J. X. Wang, N. M. Markovic, and R. R. Adzic, J. Phys. Chem. B **108**, 4127 (2004).
[33]N. M. Marković, R. R. Adžić, B. D. Cahan, and E. B. Yeager, J. Electroanal. Chem. **377**, 249 (1994).
[34]V. Stamenkovic, N. M. Markovic, and P. N. Ross, Jr., J. Electroanal. Chem. **500**, 44 (2001).
[35]R. R. Adžić, J. Wang, and B. M. Ocko, Electrochim. Acta **40**, 83 (1995).
[36]R. R. Adžić and J. X. Wang, J. Phys. Chem. B **104**, 869 (2000).
[37]M. Alvarez-Rizatti and K. Jüttner, Electrochim. Acta **33**, 33 (1988).
[38]A. Zwetanova and K. Jüttner, J. Electroanal. Chem. **119**, 149 (1981).
[39]T. J. Schmidt, U. A. Paulus, H. A. Gasteiger, and R. J. Behm, J. Electroanal. Chem. **508**, 41 (2001).
[40]D. S. Strmcnik, P. Rebec, M. Gaberscek, D. Tripkovic, V. Stamenkovic, C. Lucas, and N. M. Marković, J. Phys. Chem. C **111**, 18672 (2007).
[41]S. Beckord, S. Brimaud, and R. J. Behm, J. Electroanal. Chem. **819**, 401 (2017).
[42]V. R. Stamenkovic, B. Fowler, B. S. Mun, G. Wang, P. N. Ross, C. A. Lucas, and N. M. Marković, Science **315**, 493 (2007).
[43]J. Clavilier, D. Armand, S. G. Sun, and M. Petit, J. Electroanal. Chem. **205**, 267 (1986).
[44]C. Korzeniewsky, V. Climent, and J. M. Feliu, in *Electroanalytical Chemistry: A Series of Advances: Volume 24*, edited by A. J. Bard and C. G. Zoski (CRC Press, Boca Raton, 2012), Chap. 2, pp. 75–170.
[45]B. D. Cahan and H. M. Villullas, J. Electroanal. Chem. **307**, 263 (1991).
[46]C. K. Rhee and D.-K. Kim, J. Electroanal. Chem. **506**, 149 (2001).
[47]W. P. Zhou, L. A. Kibler, and D. M. Kolb, Electrochim. Acta **47**, 4501 (2002).
[48]C. K. Rhee, C. Jung, and B. Ku, J. Solid State Electrochem. **9**, 247 (2004).
[49]N. Garcia-Araez, V. Climent, and J. Feliu, J. Phys. Chem. C **113**, 9290 (2009).
[50]A. M. Gómez-Marín and J. M. Feliu, ChemSusChem **6**, 1091 (2013).
[51]V. Briega-Martos, E. Herrero, and J. M. Feliu, Electrochem. Commun. **85**, 32 (2017).
[52]V. Briega-Martos, E. Herrero, and J. M. Feliu, Electrochim. Acta **241**, 497 (2017).
[53]A. M. Gómez-Marín, J. M. Feliu, and E. A. Ticianelli, ACS Catal. **9**, 2238 (2019).
[54]A. M. Gómez-Marín and J. M. Feliu, Curr. Opin. Electrochem. **9**, 166 (2018).
[55]V. Briega-Martos, E. Herrero, and J. M. Feliu, Electrochim. Acta **334**, 135452 (2020).
[56]A. M. Gómez-Marín, J. Feliu, and E. A. Ticianelli, ACS Catal. **8**, 7931 (2018).
[57]A. M. Gómez-Marín and E. A. Ticianelli, Curr. Opin. Electrochem. **9**, 129 (2018).
[58]A. Malek and M. H. Eikerling, Electrocatalysis **9**, 370 (2018).
[59]Z. Su, V. Climent, J. Leitch, V. Zamlynny, J. M. Feliu, and J. Lipkowski, Phys. Chem. Chem. Phys. **12**, 15231 (2010).